

PRELIMINARY DESIGN OF POWER CONTROL STRATEGIES FOR THE HYBRID-ELECTRIC PROPULSION SYSTEM OF A LIGHTWEIGHT FIXED-WING UAV

Gianpietro Di Rito¹, Aleksander Suti¹

¹ Università di Pisa, Dipartimento di Ingegneria Civile ed Industriale, Largo Lucio Lazzarino 2, 56122 Pisa (IT)

Abstract

This paper deals with the design of power control strategies for the hybrid electric propulsion system of lightweight fixed-wing UAVs for long-endurance surveillance missions. Using as reference application a UAV with conventional thermal propulsion, the basic objective of the work is to substantiate the feasibility of its hybrid conversion, up to overcome the limitation of climb performances due to the engine overheating as well as to enhance the propulsion efficiency. Thanks to a control electronic box dedicated to the power management, the UAV electric generator is temporarily switched into motor operation, reducing the thermal engine power request, and thus avoiding its overheating. The paper demonstrates that a management of propulsion system commands (engine throttle and motor current) based on dynamic ideal-decoupling techniques is effective to track a target performance signal (as a relevant case, the engine efficiency has been selected in the work), while limiting the transient deviations of propeller speed, i.e. the UAV thrust.

Keywords: power management, hybrid propulsion, fixed-wing UAV, Optimal Operating Line

1. Introduction

The market of unmanned aerial vehicles, though the dramatic economic impact of the COVID-19 pandemic, has kept on growing through the last decades, reaching a 17.54% compound annual growth rate from 2020 to 2023 [1], [2]. The absence of CO2-emissions, the minimal noise levels. the reduced thermal signature, the high power efficiency together with the constant design improvements of energy storage devices make the electric propulsion the reference solution for lightweight UAVs in the long-term perspective. However, the specific energy of battery packs is currently much lower than that of liquid hydrocarbon fuels [2], [3] and the use of Internal Combustion Engines (ICEs) is nowadays unavoidable, especially for long-endurance UAV applications. Nevertheless, the poor thermal efficiency of ICEs, ranging from 30% to 40% [4], remains a relevant shortcoming. Hence, driven by the enhancements of electric systems efficiency as well as on the wave of the emissions goals set by ICAO, Hybrid Electric Propulsion Systems (HEPSs) are expected to play a key role in next future UAV developments, and in particular for long-endurance applications [5]. The HEPS combines the high power efficiency of electric motors with the high specific energy of fossil fuels and they could enhance both cruise and climb performances of UAVs [6]. An extensive survey on HEPS architectures for aircrafts is carried out by Wall and Meyer in [5], and relevant analyses on control strategies are proposed by Harmon in [7] and Hiserote in [8]. In particular, Hugo and Gonzalez demonstrated in [6] that, in fixed-wing UAVs, a HEPS with parallel configuration can lead to a 6.5% fuel saving, and the feasibility of this target has been recently supported by Xie et al. [9], who developed a HEPS control technique for the Rotron UAV leading to 7% fuel saving. Another advantage given by HEPSs is that the climb performances would be not limited by the ICE overheating. Actually, being the ICEs for longendurance UAVs optimized for cruise operations (i.e. at low power rating), they are typically prone to overheating during climb, when the power request significantly increases. In [10], it is pointed that the temperature rate of the ICE head of a lightweight fixed-wing UAV can exceed 1°C per second during climb.

These limitations are overcome by performing repeated small climbs alternated with levelled flights, to cool down the ICE, but the resulting performances are poor. The problem could be solved by converting conventional ICE-based systems into HEPSs. By using a control electronic box dedicated to the power control management, the UAV electric generator could be temporarily switched into motor operation, up to reduce the power delivered by the ICE, thus avoiding its overheating. In previous works by the authors [10], [11], the benefits of converting conventional ICE-based propulsion systems for UAVs into HEPSs have been preliminary demonstrated via simulations and experiments on isolated equipment, using as reference application the Rapier X-25 UAV developed by Sky Eye Systems (Italy) [12].

On the wave of these promising results and aiming to the development of a virtual prototype of the HEPS for the system validation, the research now entails the design of optimal power control strategies [13], to be defined with the following objectives:

- limitation of ICE temperature during climb;
- optimization of ICE efficiency.

2. System description

The HEPS is essentially composed of (Figure 1, additional elements with respect to the ones already installed on the UAV are indicated in red):

- a two-stroke single-cylinder ICE with related Engine Control Unit (ECU) [14]
- a three-phase Brush-Less DC Machine (BLDCM), i.e. Electric Machine (EM) [15];
- an EM ECU, implementing a closed-loop current control when the EM acts as a motor;
- a belt-pulleys mechanical transmission to let ICE and EM work in parallel (i.e., torquesumming) arrangement;
- a twin-blade fixed-pitch propeller [16] mounted on the ICE output shaft;
- a Main Battery pack [17] for the power supply of on-board systems and ICE ECU during hybrid (and emergency) operations;
- a EM Battery pack [17] for the power supply of the EM during hybrid operations;
- a HEPS ECU, implementing the power control strategies.

The HEPS can provide power to the UAV propeller in conventional configuration (the ICE delivers power to propeller and EM, working as generator) as well as in hybrid configuration (in which the propeller is powered by both ICE and EM, working as booster motor and supplied by the EM battery). In particular, depending on the EM working conditions and EM battery, the following operation modes are defined:

- Generator Mode/Battery Disengaged (GM/BD), in which the EM battery has reached a pre-defined state of charge and it is disengaged from the EM;
- Generator Mode/Battery Engaged (GM/BE), in which the EM battery is charging, and it represents an electrical load for the EM;
- Booster Mode (BM), in which the EM, powered by the EM battery, works as motor and delivers torque on the propeller shaft, therefore supporting the ICE in the generation of the UAV thrust.

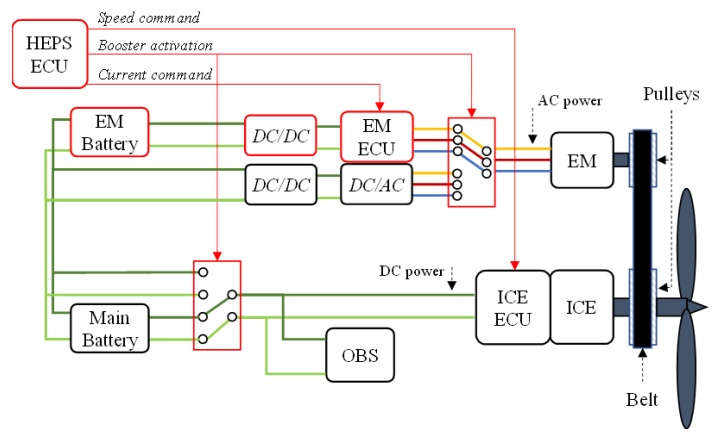


Figure 1 – HEPS architecture (the connections are related to "Booster Mode" operation).

3. Propulsion system dynamic model

3.1 Aeromechanical section

The mechanical transmission dynamics is modelled via (1), [10]:

$$\begin{cases} J_{ice}\dot{\omega}_{ice} = Q_{ice}(\omega_{ice}, \delta_t) - Q_p(\omega_{ice}, AR) - r_{ice}(C_b\dot{\varepsilon} + K_b\varepsilon) \\ J_{em}\dot{\omega}_{em} = r_{em}(C_b\dot{\varepsilon} + K_b\varepsilon) - Q_{em} \\ \dot{\varepsilon} = r_{ice}\omega_{ice} - r_{em}\omega_{em} \\ Q_p = C_Q(\omega_p, AR)\rho D_p^5\omega_{ice}^2 \end{cases} , \tag{1}$$

in which ω_{ice} and ω_{em} are the ICE and EM angular speeds, J_{ice} and J_{em} are the shaft inertias, r_{ice} and r_{em} are the pulley radii, Q_{ice} is the ICE torque (depending on ICE speed and throttle δ_t , Figure 2(Left)), Q_p is the propeller torque, C_Q is the propeller torque coefficient (depending on propeller speed and advance ratio AR, Figure 2 (Right)), D_p is the propeller diameter, ρ is the air density, V_a is the forward UAV speed, Q_{em} is the EM torque, K_b and C_b are the belt stiffness and damping, ε and $\dot{\varepsilon}$ are the belt deformation and deformation rate respectively.

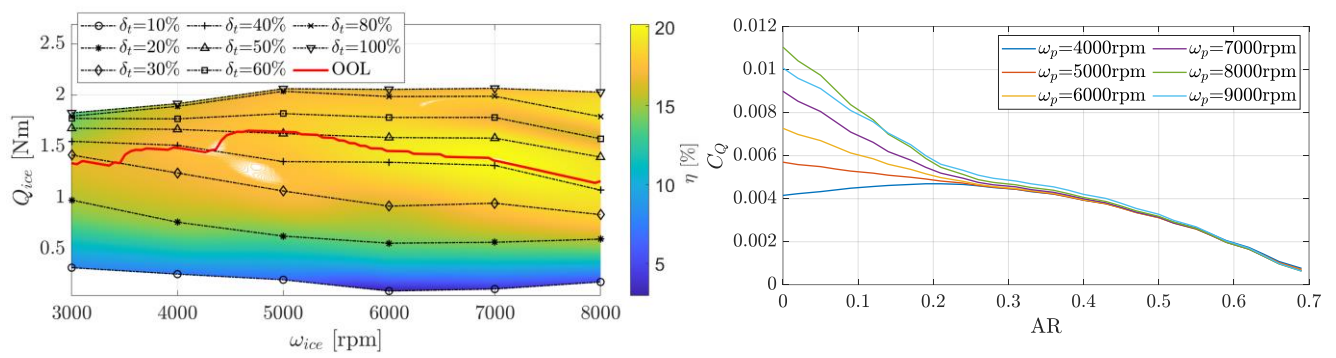


Figure 2 – (Left) ICE torque map; (Right) APC 18x8 propeller torque coefficient.

3.2 Electric machine section

The current dynamics of the reference EM, which is a BLDCM, can be expressed in a vectorized form by Eq.(2),[11], Figure 3:

$$\begin{cases} V_{abc} = R I_{abc} + L \dot{I}_{abc} + E_{abc} (n_d \theta_{em}) \\ E_{abc} = k_m \dot{\theta}_{em} e_{abc} \end{cases}$$
(2)

in which $\mathbf{V}_{abc} = [V_a - V_n, V_b - V_n, V_c - V_n]^T$ is the applied voltages vector, $\mathbf{I}_{abc} = [I_a, I_b, I_c]^T$ is the stator currents vector, \mathbf{E}_{abc} is the Back Electro-Motive Force (BEMF) vector, R and L are the resistance and inductance of the phases, k_m is the motor speed constant, $\mathbf{e}_{abc} = [e_a, e_b, e_c]^T$ is the BEMF waveforms vector.

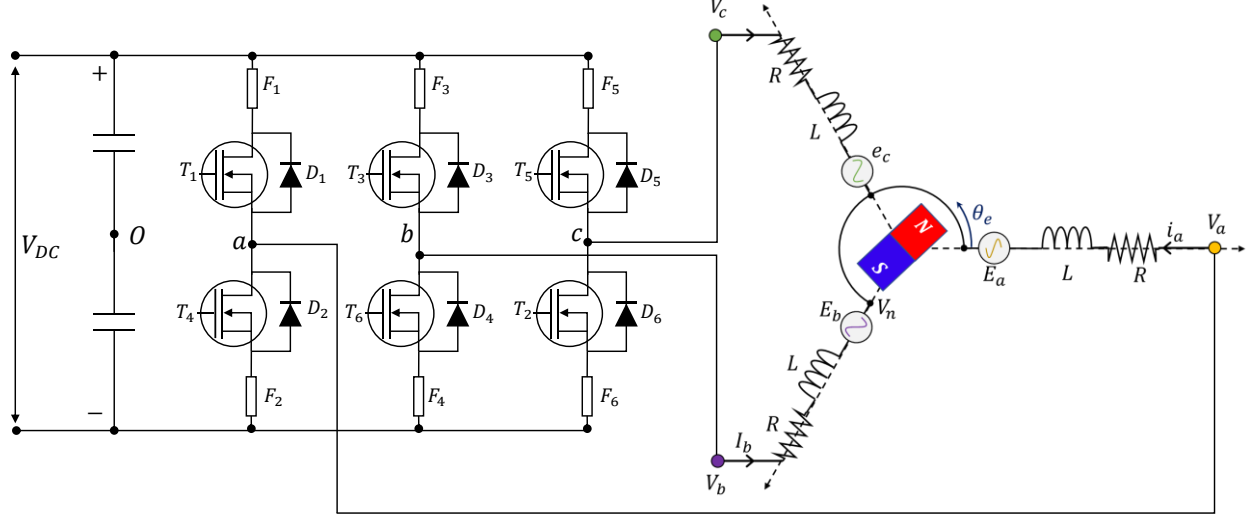


Figure 3 - Schematics of the BLDCM (one pole pair) driven by a three-leg converter.

Since the EM is driven via a six-step commutation logic, the three-phase model in Eq.(2) can be

expressed through a scalar monophase equivalent model [16], as in Eq.(3)

$$V_{em} = 2RI_{em} + 2L\dot{I}_{em} + 2k_m\dot{\theta}_{em}.$$
 (3)

The electromagnetic torque can be then expressed by Eq.(4):

$$Q_{em} = \frac{1}{\dot{\theta}_{em}} \mathbf{I}_{abc} \cdot \mathbf{E}_{abc} = 2k_m I_{em}. \tag{4}$$

3.3 Battery packs and on-board systems sections

The current dynamics of the reference battery pack have been modelled with reference to Figure 4 via Thevenin-based equivalent circuit model, Eq.(5), [18]:

$$\begin{cases} V_{b} = V_{OC}(SOC, T_{b}) - R_{0}(SOC, T_{b})\dot{Q}_{b} - \sum_{j=1}^{2} V_{j} \\ SOC = SOC_{0} - 1/Q_{btot} \int_{0}^{t} \dot{Q}_{b} dt \\ \dot{V}_{j} = \dot{Q}_{b}/C_{j}(SOC, T_{b}) - V_{j}/R_{j}(SOC, T_{b})C_{j}(SOC, T_{b}) \end{cases}$$
(5)

where Q_b is the electrical charge (i.e., SOC), \dot{Q}_b is the delivered current, V_{OC} is the Open Circuit Voltage and R_0 is the internal resistance, while R_j and C_j are the resistance and the capacitance of the *j*-th grid, respectively.

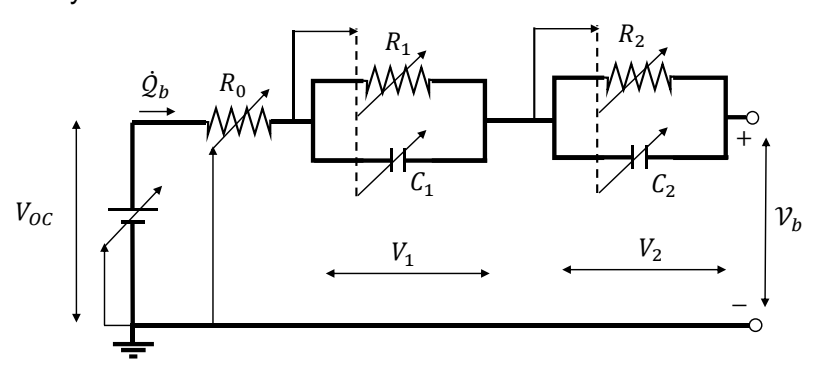


Figure 4. Thevenin equivalent circuit of the reference battery.

The literature highlights that the parameters of each element of the Thevenin circuit are mainly functions of the SOC and the battery temperature [19].

The on-board systems dynamics is instead modelled as an inductive-resistive load, in which the resistance is set as an input of the model to simulate variations of power requests, Eq.(6):

$$V_{OBS} = R_{oS}(t)I_{oS} + L_{oS}\dot{I}_{oS}, \tag{6}$$

where I_{os} is the current delivered to the on-board systems, while L_{os} and $R_{os}(t)$ are the equivalent values of inductance and resistance of the network.

4. Power control strategies

In HEPS and full-electric propulsion systems, a crucial design point is related to the energy management [20], [21]. The basic idea underlying this work is that the power control strategies implemented by the HEPS ECU during BM operations can leverage a TITO (Two-Inputs/Two-Outputs) ideal-decoupling [22], as schematically reported in Figure 5.

Once defined the inputs as the demands of EM current and ICE throttle (signals u1 and u2 in Figure 5, respectively), different types of strategies can be obtained, depending on the selected states/outputs for the scheme (signals y1 and y2 in Figure 5, respectively). As a relevant example, the HEPS can regulate the power split to track an efficiency target (e.g. ICE Optimal Operating Line (OOL), Figure 5), while maintaining the ICE speed (i.e. UAV thrust).

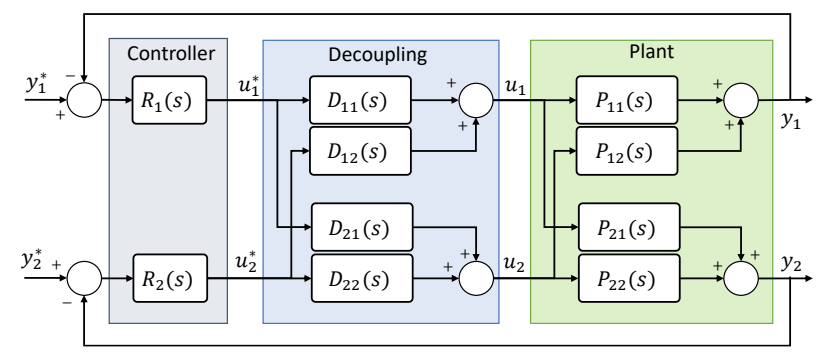


Figure 5 – HEPS control strategy based on TITO ideal-decoupling.

Based on the ideal-decoupling strategy, the decoupled process should have a diagonal transfer function matrix G(s) as showed hereafter:

$$\mathbf{G}(s) = \mathbf{P}(s)\mathbf{D}(s) = \begin{bmatrix} P_{11}(s) & P_{12}(s) \\ P_{21}(s) & P_{22}(s) \end{bmatrix} \begin{bmatrix} D_{11}(s) & D_{12}(s) \\ D_{21}(s) & D_{22}(s) \end{bmatrix} = \begin{bmatrix} P_{11}(s) & 0 \\ 0 & P_{22}(s) \end{bmatrix}$$
(7)

where D(s) is the decoupling transfer function matrix, which components can be obtained by superimposing the decoupling requirement in Eq. (7):

$$D_{11}(s) = -\frac{P_{11}P_{22}}{P_{11}P_{22} + P_{12}P_{21}}$$

$$D_{12}(s) = \frac{P_{12}P_{22}}{P_{11}P_{22} + P_{12}P_{21}}$$

$$D_{21}(s) = \frac{P_{11}P_{21}}{P_{11}P_{22} + P_{12}P_{21}}$$

$$D_{22}(s) = \frac{P_{11}P_{22}}{P_{11}P_{22} + P_{12}P_{21}}$$

$$D_{22}(s) = \frac{P_{11}P_{22}}{P_{11}P_{22} + P_{12}P_{21}}$$
(8)

5. Results

The effectiveness of the proposed power management strategies has been assessed via nonlinear simulations, in which the following sequence of events are imposed in both climb and cruise conditions (the HEPS model has been entirely developed on MATLAB/Simulink environment, and its numerical solution is obtained via the fourth order Runge–Kutta method at 10⁻⁴ s of integration time step):

- <u>Initial condition (t = 0 s)</u>: the UAV flies at 22 m/s airspeed and the HEPS works in conventional operation (GM/BD), so that the ICE drives the propeller at 7500 rpm in climb, and at 5500 rpm in cruise;
- <u>Transition to hybrid mode (*Hb On*, t = 1 s)</u>: the HEPS is switched to BM and the EM current demand is set to zero:
- Activation of the OOL strategy (OOL On, t = 2 s): the EM current demand is automatically regulated by the HEPS efficiency controller, tracking the ICE OOL.

To evaluate the impact of the decoupling strategy on the system performances, the results are hereafter proposed with and without it.

The results of the first test, with the UAV operating in climb condition, are shown in Figure 6 and Figure 7. From Figure 6 (left), it can be observed that when the OOL mode is activated, the efficiency regulator effectively tracks the OOL. Additionally, the speed oscillation caused by changes in the EM current (Figure 6 (right)) is reduced when decoupling is applied. During climb, to reach the OOL, the system operates at a speed level for which the throttle position should be reduced (Figure 6 (right)): this requires that the EM acts as a motor, which is beneficial for the ICE in terms of maximum power excess. This benefit is highlighted in Figure 7 (left), which shows the power distribution among the HEPS components. For completeness, the main responses of the EM and main battery are also plotted in Figure 7 (right).

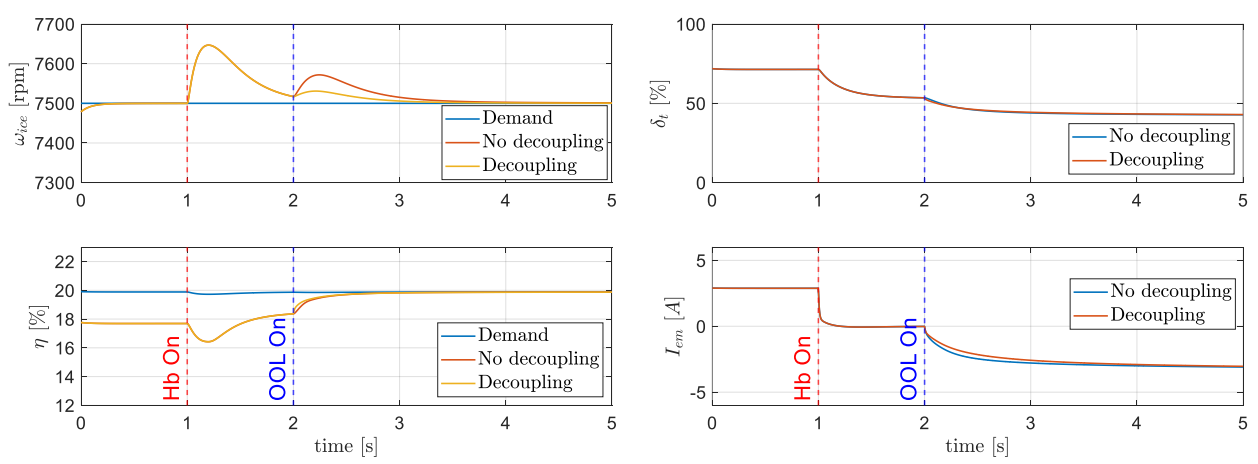


Figure 6 – Climb condition: (left) ICE speed and efficiency; (right) ICE throttle and EM current.

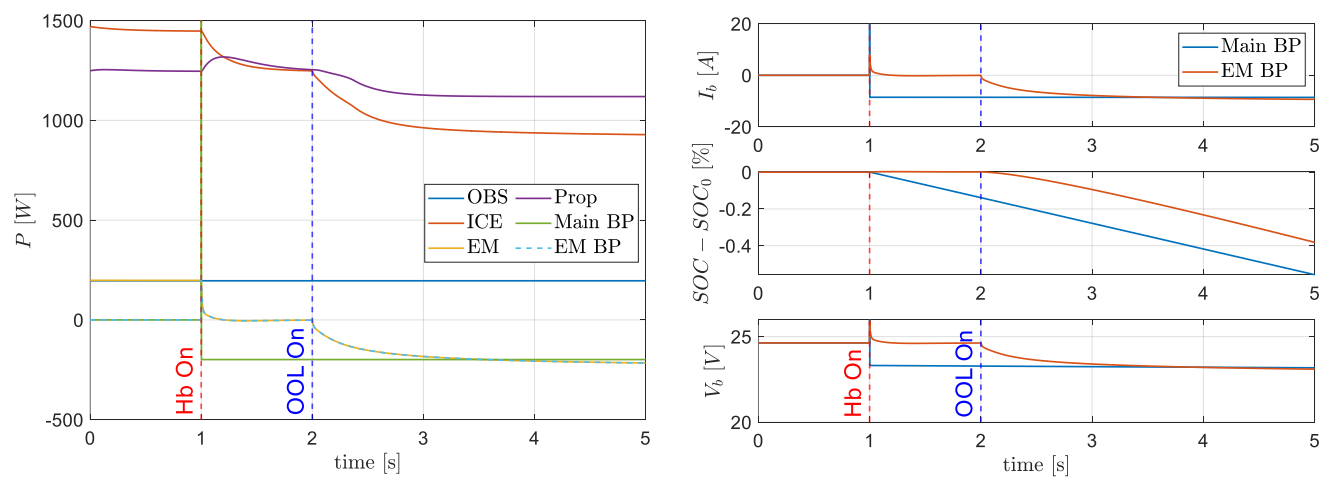


Figure 7 – Climb condition: (left) power distribution; (right) battery packs data.

The results referring to cruise condition are then shown in Figure 8 and Figure 9. When the OOL operation is activated, the efficiency regulator effectively tracks the OOL, and the speed oscillation caused by changes in the EM current (Figure 8 (right)) is minimized when decoupling is applied.

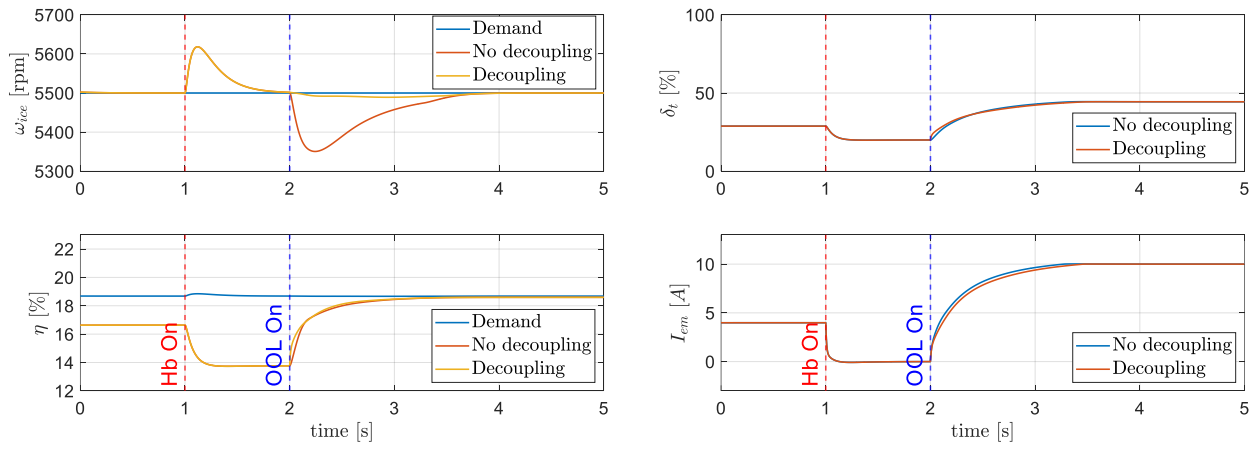


Figure 8 - Cruise condition: (left) ICE speed and efficiency; (right) ICE throttle and EM current.

During cruise, to reach the OOL, the system operates at a speed for which the throttle should be increased (Figure 8 (right)), requiring the EM to act as a brake. This can be conveniently obtained by re-charging the battery pack dedicated to the EM itself (discharged in climb). In cruise, the ICE power request is well lower than climb, permitting the ICE to deliver power without degrading its power excess. These considerations are supported by Figure 9, reporting the power distribution among components (left) and the battery packs data (right).

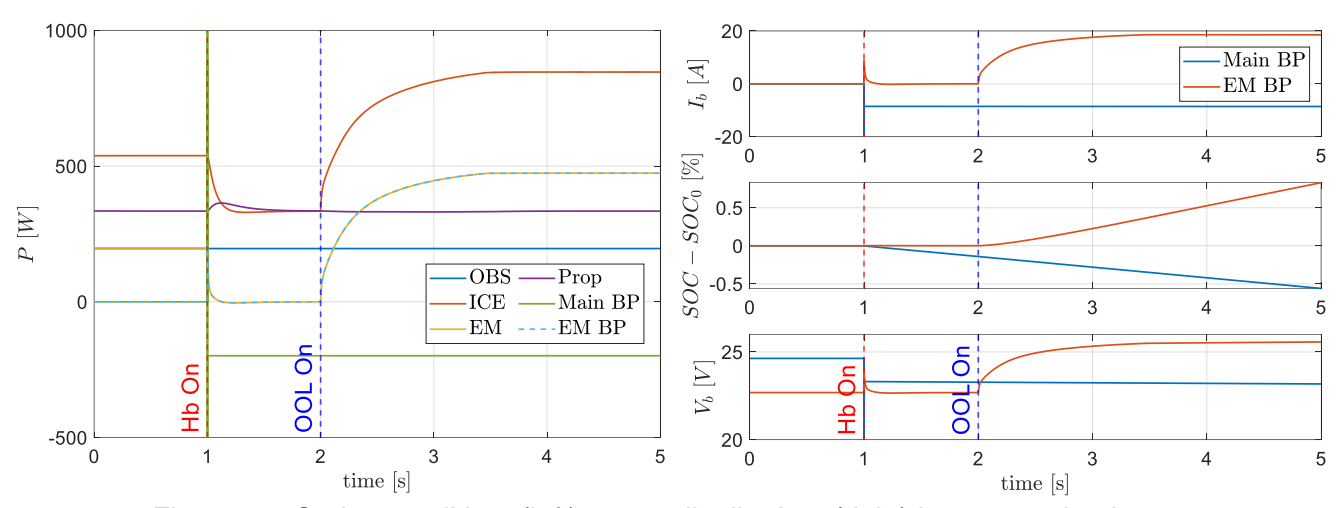


Figure 9 – Cruise condition: (left) power distribution; (right) battery packs data.

Conclusions

The work demonstrates the effectiveness of power control strategies based on ideal-decoupling techniques to manage the HEPS of a lightweight fixed-wing UAV, by using a control electronics that converts the UAV electrical generator into a booster motor for enhancing the propulsion performances. Different power management strategies can be applied when the HEPS operates in hybrid mode, also depending on mission phase: this work focuses on a strategy tracking the ICE OOL. During climb, the ICE requires to decrease throttle to reach the OOL target, so that the electric machine must work as a motor, while during cruise, it must act as a brake to let the ICE reach the OOL. These two requests can be conveniently harmonized in a climb/cruise cycle, by discharging and re-charging the battery pack dedicated to the EM itself. The results further demonstrate the effectiveness of a TITO ideal-decoupling technique to manage the ICE throttle and electric motor current demand for tracking a target signal as the ICE efficiency, while limiting transient deviations in propeller speed, i.e. the UAV thrust.

Contact Author Email Address

Mail to: gianpietro.di.rito@unipi.it

Copyright Statement

The authors confirm that they, and/or their company or organization, hold copyright on all of the original material included in this paper. The authors also confirm that they have obtained permission, from the copyright holder of any third party material included in this paper, to publish it as part of their paper. The authors confirm that they give permission, or have obtained permission from the copyright holder of this paper, for the publication and distribution of this paper as part of the ICAS proceedings or as individual off-prints from the proceedings.

References

- [1] MARKETS AND MARKETS, "UAV (Drone) Market Global Forecast to 2029." Accessed: Jun. 13, 2024. [Online]. Available: https://www.marketsandmarkets.com/Market-Reports/unmanned-aerial-vehicles-uav-market-662.html?gad_source=1&gclid=Cj0KCQjwsaqzBhDdARIsAK2gqndYZtyf5Tgxalxs74MDgAdvU 6OKwTB-I1Es9De5nw6DUclr9Z3382IaAu1KEALw_wcB
- [2] M. Mazzoleni, G. Di Rito, and F. Previdi, *Electro-Mechanical Actuators for the More Electric Aircraft*. Cham: Springer International Publishing, 2021. doi: 10.1007/978-3-030-61799-8.
- [3] J. Van Mierlo *et al.*, "Beyond the State of the Art of Electric Vehicles: A Fact-Based Paper of the Current and Prospective Electric Vehicle Technologies," *World Electric Vehicle Journal*, vol. 12, no. 1, p. 20, Feb. 2021, doi: 10.3390/wevi12010020.
- [4] A. Bhatia, A. Mendiratta, and M. Vaish, "Notice of Retraction: Comparison of proposed six stroke internal combustion engine with four stroke engine using ideal cycle," in 2010 2nd International Conference on Mechanical and Electronics Engineering, IEEE, Aug. 2010, pp. V1-222-V1-225. doi: 10.1109/ICMEE.2010.5558559.
- [5] T. J. Wall and R. Meyer, "A Survey of Hybrid Electric Propulsion for Aircraft," in *53rd AIAA/SAE/ASEE Joint Propulsion Conference*, Reston, Virginia: American Institute of

- Aeronautics and Astronautics, Jul. 2017. doi: 10.2514/6.2017-4700.
- [6] J. Y. Hung and L. F. Gonzalez, "On parallel hybrid-electric propulsion system for unmanned aerial vehicles," *Progress in Aerospace Sciences*, vol. 51, pp. 1–17, May 2012, doi: 10.1016/j.paerosci.2011.12.001.
- [7] F. G. Harmon, A. A. Frank, and J.-J. Chattot, "Conceptual Design and Simulation of a Small Hybrid-Electric Unmanned Aerial Vehicle," *J Aircr*, vol. 43, no. 5, pp. 1490–1498, Sep. 2006, doi: 10.2514/1.15816.
- [8] R. Hiserote and F. Harmon, "Analysis of Hybrid-Electric Propulsion System Designs for Small Unmanned Aircraft Systems," in 8th Annual International Energy Conversion Engineering Conference, Reston, Virigina: American Institute of Aeronautics and Astronautics, Jul. 2010. doi: 10.2514/6.2010-6687.
- [9] Y. Xie, A. Savvaris, A. Tsourdos, J. Laycock, and A. Farmer, "Modelling and control of a hybrid electric propulsion system for unmanned aerial vehicles," in *2018 IEEE Aerospace Conference*, IEEE, Mar. 2018, pp. 1–13. doi: 10.1109/AERO.2018.8396436.
- [10] A. Suti, G. Di Rito, and R. Galatolo, "Climbing performance enhancement of small fixed-wing UAVs via hybrid electric propulsion," in 2021 IEEE Workshop on Electrical Machines Design, Control and Diagnosis (WEMDCD), IEEE, Apr. 2021, pp. 305–310. doi: 10.1109/WEMDCD51469.2021.9425638.
- [11] G. Di Rito, A. Suti, A. Ricci, R. Galatolo, and G. Mattei, "Experimental characterisation of Li-Po battery packs and BLDC machines for hybrid propulsion systems of lightweight UAVs," in 2022 IEEE 9th International Workshop on Metrology for AeroSpace (MetroAeroSpace), IEEE, Jun. 2022, pp. 49–53. doi: 10.1109/MetroAeroSpace54187.2022.9856056.
- [12] "Sky Eye Systems, RAPIER X-SKYSAR. Available at: https://www.skyeyesystems.it/products/rapier-x-skysar/ (Accessed on 15 September 2023)."
- [13] M. Doff-Sotta, M. Cannon, and M. Bacic, "Optimal energy management for hybrid electric aircraft," *IFAC-PapersOnLine*, vol. 53, no. 2, pp. 6043–6049, 2020, doi: 10.1016/j.ifacol.2020.12.1672.
- [14] "Currawong Engineering, Corvid-29." Accessed: Oct. 15, 2023. [Online]. Available: https://www.currawongeng.com/corvid-29/
- [15] "Maxon, view product, motor." Accessed: Oct. 15, 2023. [Online]. Available: https://www.maxongroup.it/maxon/view/product/motor/ec4pole/305015
- [16] "APC Propellers TECHNICAL INFO." Accessed: May 10, 2023. [Online]. Available: https://www.apcprop.com/technical-information/performance-data/
- [17] "Maxamps Lithium Batteries, LiPo 1850 6S 22.2v Battery Pack." Accessed: Oct. 15, 2023. [Online]. Available: https://maxamps.com/products/lipo-1850-6s-22-2v-battery-pack
- [18] A. Suti, G. Di Rito, and G. Mattei, "Development and Experimental Validation of Novel Thevenin-Based Hysteretic Models for Li-Po Battery Packs Employed in Fixed-Wing UAVs," *Energies (Basel)*, vol. 15, no. 23, p. 9249, Dec. 2022, doi: 10.3390/en15239249.
- [19] A. Suti, G. Di Rito, and G. Mattei, "Heuristic Estimation of Temperature-Dependant Model Parameters of Li-Po Batteries for UAV Applications," in 2023 IEEE 10th International Workshop on Metrology for AeroSpace (MetroAeroSpace), IEEE, Jun. 2023, pp. 269–274. doi: 10.1109/MetroAeroSpace57412.2023.10190045.
- [20] F. Schettini, E. Denti, and G. Di Rito, "Development of a simulation platform of all-electric aircraft on-board systems for energy management studies," *The Aeronautical Journal*, vol. 121, no. 1239, pp. 710–719, May 2017, doi: 10.1017/aer.2017.16.
- [21] F. Schettini, E. Denti, G. Di Rito, and R. Galatolo, "Simulation of an all-electric flight control system for the evaluation of power consumption," in *29th Congress of the International Council of the Aeronautical Sciences, ICAS 2014*, St. Petersburg; Russian Federation: International Council of the Aeronautical Sciences, Sep. 2014.
- [22] Z. Li and Y. Chen, "Ideal, Simplified and Inverted Decoupling of Fractional Order TITO Processes," *IFAC Proceedings Volumes*, vol. 47, no. 3, pp. 2897–2902, 2014, doi: 10.3182/20140824-6-ZA-1003.02107.